Commissioning of the MIGDAL detector with fast neutrons

Tim Marley

Imperial College London

On behalf of the MIGDAL Collaboration

DMUK Meeting January 2025 - KCL

The Migdal effect

- Direct DM experiments invoke the Migdal effect to probe energies below their nuclear recoil threshold.
- Predicted by A. Migdal in the 1930s/1940s and first observed in radioactive decays in the 1970s – but not yet recorded in nuclear scattering.
- Migdal In Galactic Dark mAtter expLoration (MIGDAL) Experiment
  - We aim to achieve the unambiguous observation (and characterisation) of the Migdal effect using a low-pressure optical TPC and high-energy neutrons.

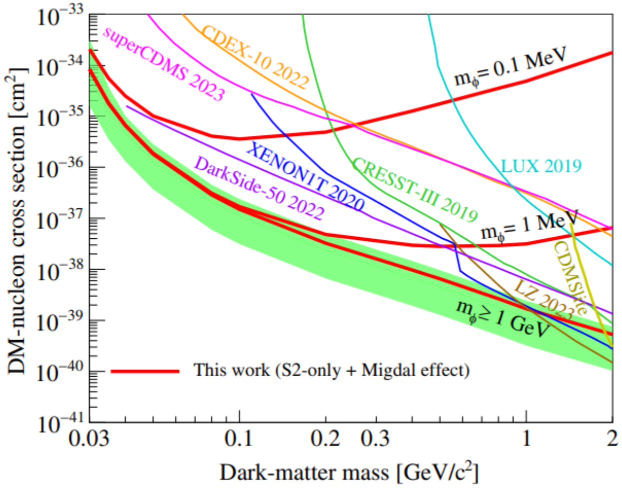

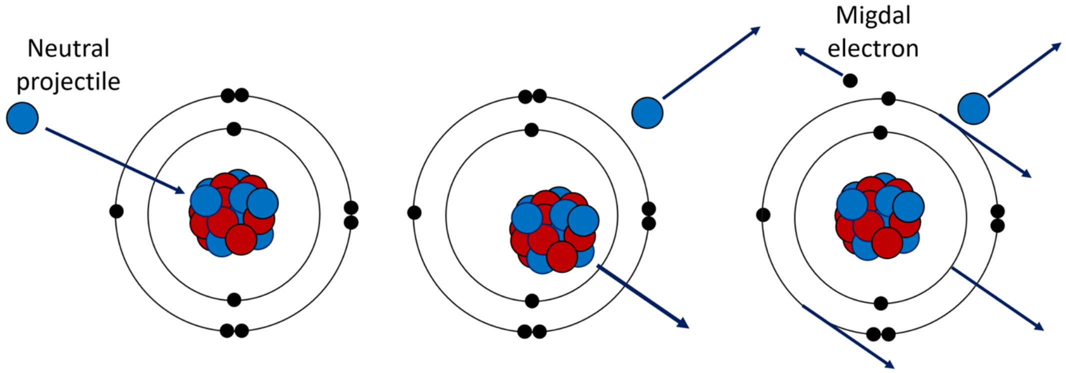

Migdal topology involves an electron and a nuclear recoil originating from the same vertex.

The MIGDAL Experiment

- High-yield neutron generator
  - D-D: 2.47 MeV (10^9 n/s)
  - Defined, collimated beam
- Low-pressure gas: 50 Torr of CF_4
  - Visible light + VUV scintillator
  - Extended particle tracks, Long attenuation length for gamma rays
  - Can add fraction of noble gases relevant to dark matter searches (Ar / Xe)
- Optical TPC
  - Amplification: 2x glass-GEMs
  - Optical: camera + photomultiplier tube
  - Charge: 120 ITO anode strips
- Electron and nuclear recoil tracks
  - Migdal: NR+ER tracks, common vertex
  - NR and ER tracks have opposite dE/dx profiles
  - 5 keV electron threshold (^{55}Fe calibration)

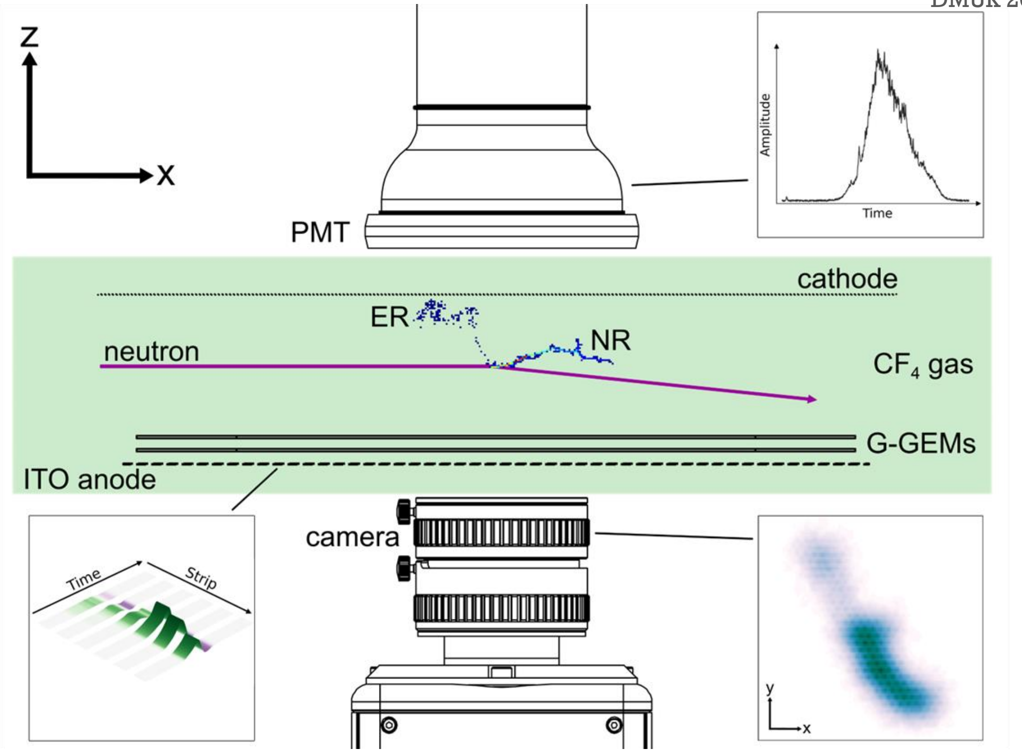

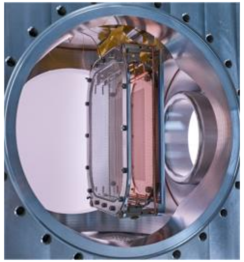

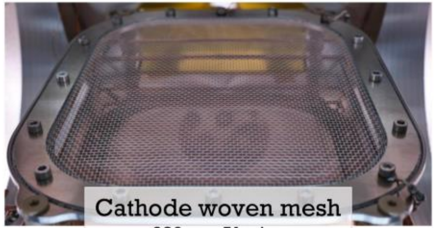

Cathode woven mesh
280 µm Al wire

Double glass-GEMs
Diameter: 170 µm | pitch: 280 µm | thickness: 570 µm

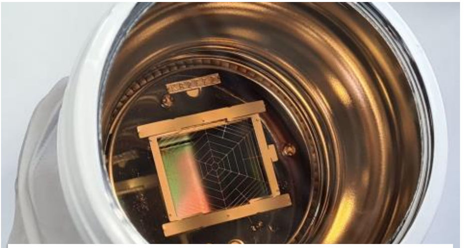

Hamamatsu R11410 PMT (trigger)

Combining optical and charge readout

EHD f/0.85 25 mm lens

ORCA Quest

- Low-noise qCMOS camera
- RMS noise:
  - 0.41e⁻ @ 120 Hz
  - 0.21e⁻ @ 5 Hz
- 12-bit resolution

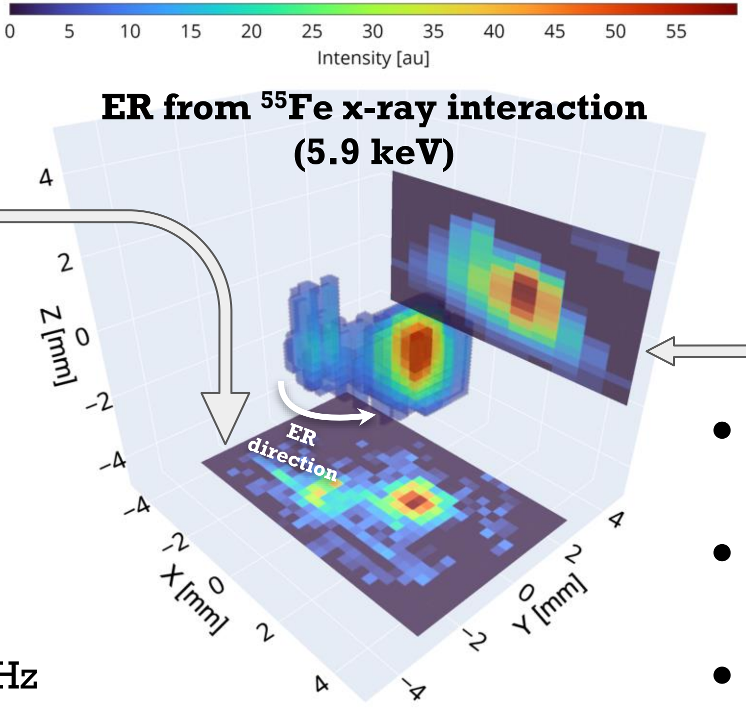

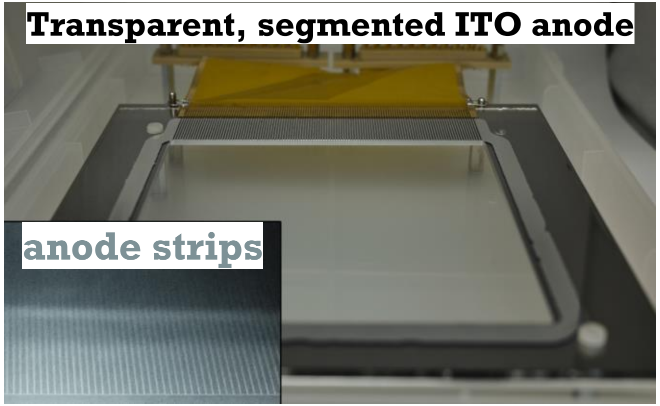

120 strips

- 120 strips connected to 60 fast commercial amplifiers (LMH6629)
- 0.6 mm strips with 0.8 mm pitch, 10 cm x 10 cm active area
- Digitised with 2 ns sampling rate at 8-bit resolution with Acqiris DAQ

NILE facility at Rutherford Appleton Laboratory, UK

- Bespoke DD and DT neutron irradiation facility located within Target Station 2 at ISIS Neutron and Muon Source, RAL
- Concrete bunker with interlocked access
- MIGDAL experiment sits in the centre of the bunker

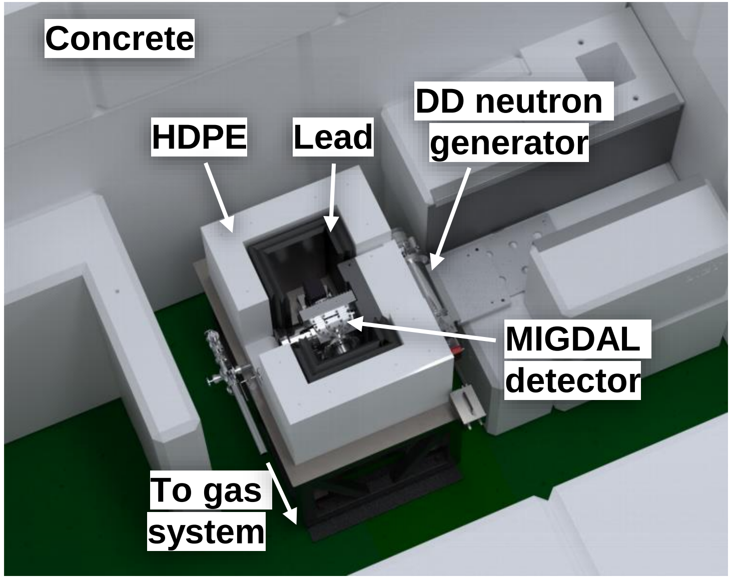

Shielded and unshielded renders of the experiment

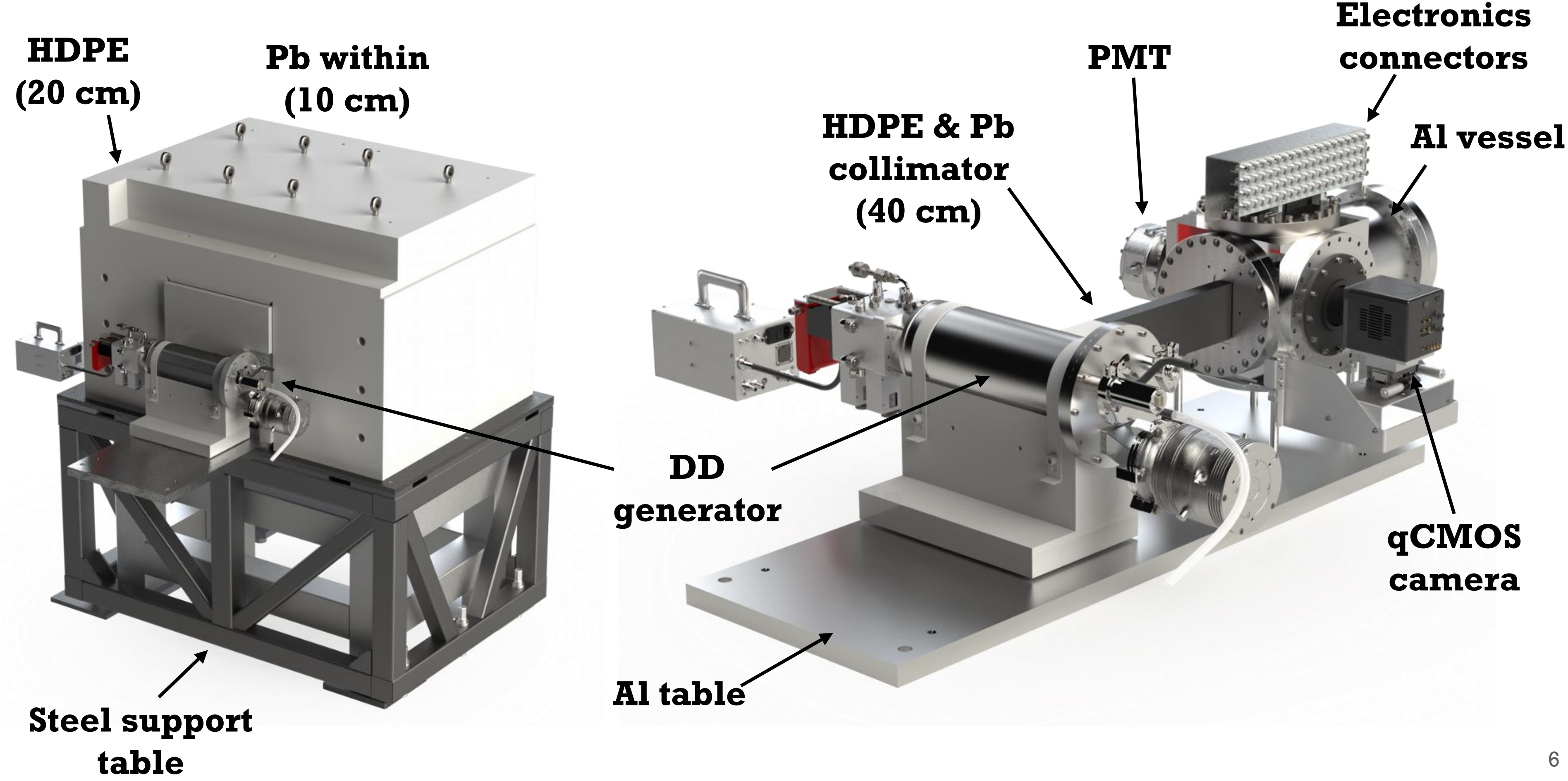

Characterising the neutron and NR rate

- Expected **2.6×10^5 n/s** entering the active volume, but measured **6×10^4 n/s**.
- Our collimator was designed around an **8 mm** neutron production spot diameter within the DD generator, but the measured diameter was much closer to **25 mm**.
- This reduced the NR event rate in the active volume from **~15 Hz** to **~5 Hz**.
- The camera was pulled closer to the active volume to capture more light.
  - This further reduced the contained NR rate in the ROI to **~2 Hz**, which we observe in the data.

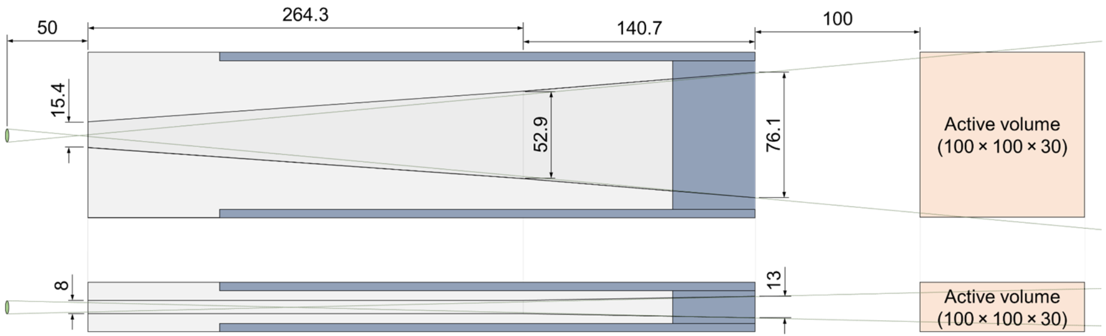

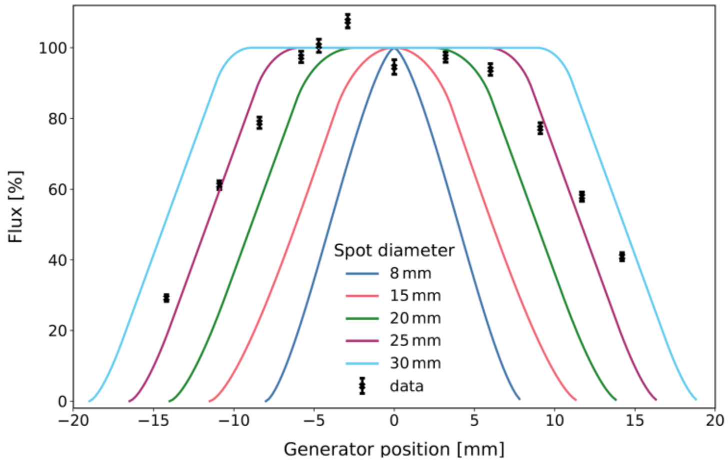

Science operations

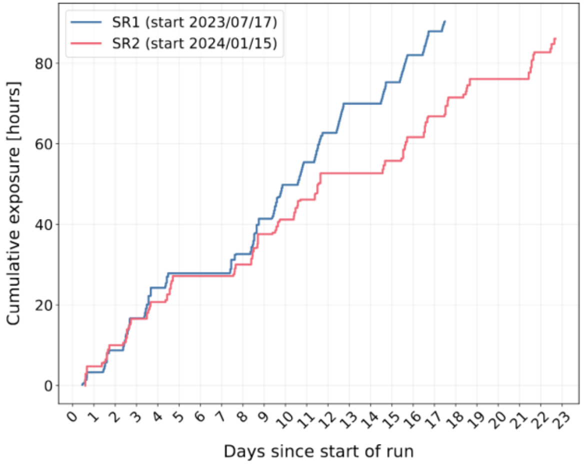

- First science run
  - 17/07/23 – 03/08/23
- Second science run
  - 15/01/24 – 06/02/24
- Data taken using D-D neutron generator recorded continuously during 10-hour long shifts.
  - 50% of our data remains blinded.
  - Approximately 500,000 NRs in total.
- Calibration runs with ^{55}Fe every 3 hours.
- We replaced the gas medium once/twice per week.

Summary of gain and gain resolution over the course of first science run.

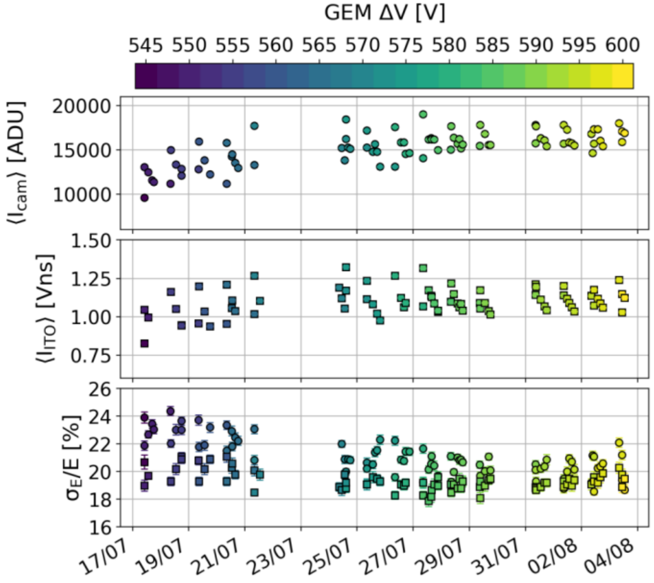

Backgrounds

- We do not expect to be limited by background.
  - We wanted to confirm this by measuring the sideband outside the energy and spatial ROI.
- **Secondary NRs** could create a split topology, similar to Migdal.
  - We can exclude these with kinematic and parametric constraints.
- **Compton scatters** of **γ-rays** from **neutron inelastic scattering** can create events with NR + ER.
  - This is the main source of background.

(Astropart. Phys. 151 (2023) 102853)

Component	Topology	D-D neutrons >0.5	5–15 keV
Recoil-induced δ-rays	Delta electron from NR track origin	≈0	0
Particle-Induced X-ray Emission (PIXE)			
X-ray emission	Photoelectron near NR track origin	1.8	0
Auger electrons	Auger electron from NR track origin	19.6	0
Bremsstrahlung processes†			
Quasi-Free Electron Br. (QFEB)	Photoelectron near NR track origin	112	≈0
Secondary Electron Br. (SEB)	Photoelectron near NR track origin	115	≈0
Atomic Br. (AB)	Photoelectron near NR track origin	70	≈0
Nuclear Br. (NB)	Photoelectron near NR track origin	≈0	≈0
Neutron inelastic γ-rays	Compton electron near NR track origin	1.6	0.47
Random track coincidences			
External γ- and X-rays	Photo-/Compton electron near NR track	≈0	≈0
Trace radioisotopes (gas)	Electron from decay near NR track origin	0.2	0.01
Neutron activation (gas)	Electron from decay near NR track origin	0	0
Muon-induced δ-rays	Delta electron near NR track origin	≈0	≈0
Secondary nuclear recoil fork	NR track fork near track origin	–	≈1
Total background	Sum of the above components		1.5
Migdal signal	Migdal electron from NR track origin		32.6

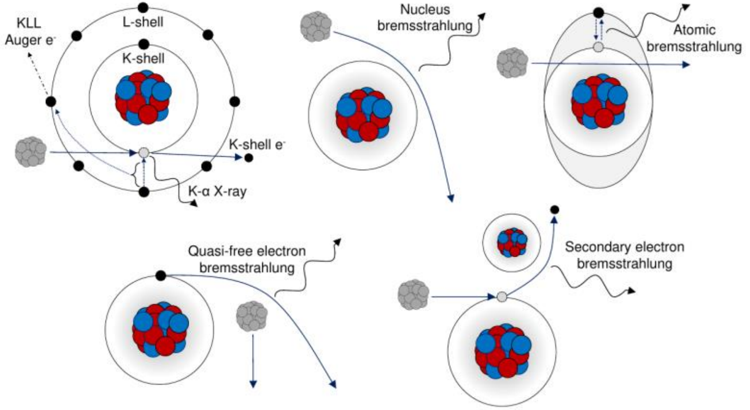

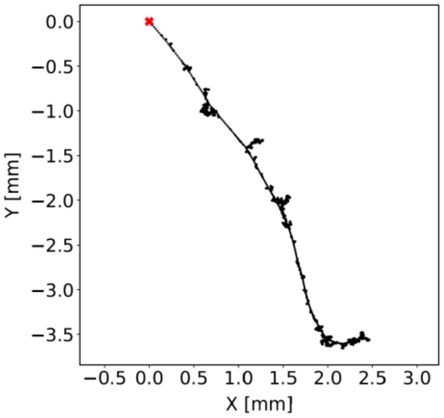

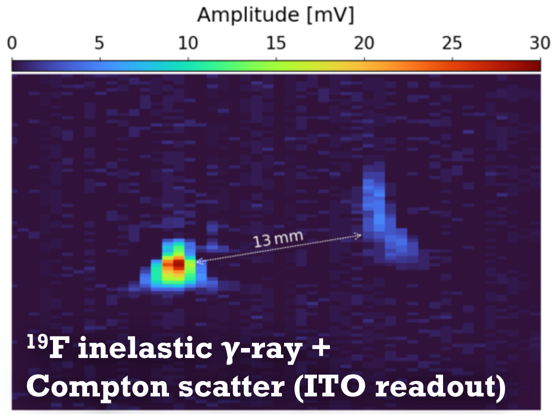

Backgrounds

- We do not expect to be limited by background.
  - We wanted to confirm this by measuring the sideband outside the energy and spatial ROI.
- **Secondary NRs** could create a split topology, similar to Migdal.
  - We can exclude these with kinematic and parametric constraints.
- **Compton scatters** of **γ-rays** from **neutron inelastic scattering** can create events with NR + ER.
  - This is the main source of background.

[(Astropart. Phys. 151 (2023) 102853)]

Component	Topology	D-D neutrons >0.5	D-D neutrons 5–15 keV
Recoil-induced δ-rays	Delta electron from NR track origin	≈0	0
Particle-Induced X-ray Emission (PIXE)			
X-ray emission	Photoelectron near NR track origin	1.8	0
Auger electrons	Auger electron from NR track origin	19.6	0
Bremss[illegible]			
Quasi-Free Electron Br. (QFEB)	Photoelectron near NR track origin	112	≈0
Secondary Electron Br. (SEB)	Photoelectron near NR track origin	115	≈0
Atomic Br. (AB)	Photoelectron near NR track origin	70	≈0
Nuclear Br. (NB)	Photoelectron near NR track origin	≈0	≈0
Neutron inelastic γ-rays	Compton electron near NR track origin	1.6	0.47
Random track coincidences			
External γ- and X-rays	Photo-/Compton electron near NR track	≈0	≈0
Trace radi[illegible]	[illegible]	[illegible]	0.01
Neutron activation (gas)	Electron from decay near NR track origin	0	0
Muon-induced δ-rays	Delta electron near NR track origin	≈0	≈0
Secondary nuclear recoil fork	NR track fork near track origin	–	≈1
Total background	Sum of the above components		1.5
Migdal signal	Migdal electron from NR track origin		32.6

Eliminated by applying an energy threshold

Eliminated by ITO timing resolution

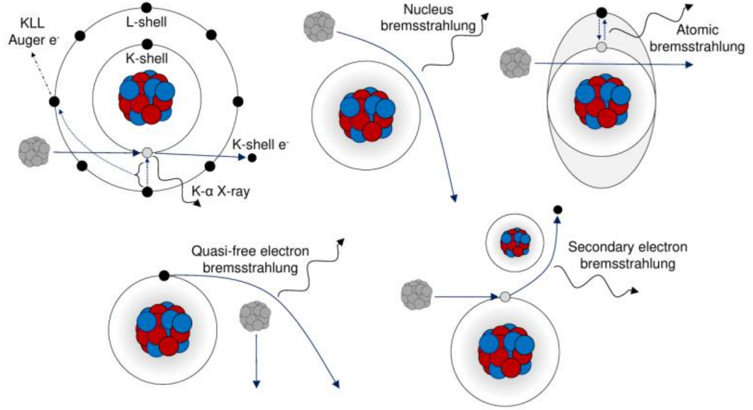

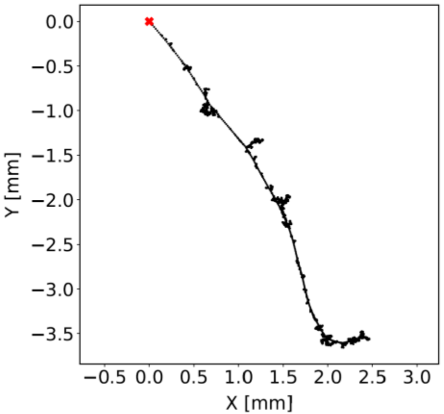

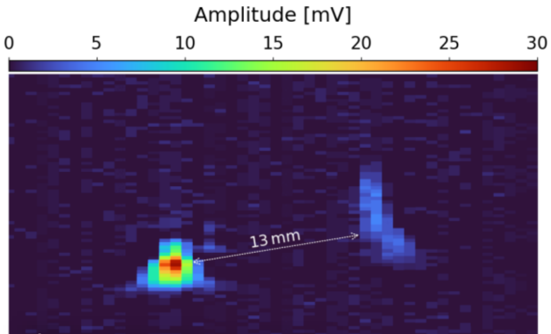

^{19}F inelastic γ-ray + Compton scatter (ITO readout)

Measuring the neutron inelastic γ-ray sideband

- We have constructed a detailed GEANT4 detector geometry to calculate the expected number of γ-rays.
- The number of simulated and measured NR + ER coincidences is consistent.
- The expected (and measured) number of ERs produced within 3 mm of an NR vertex is very small (good news).

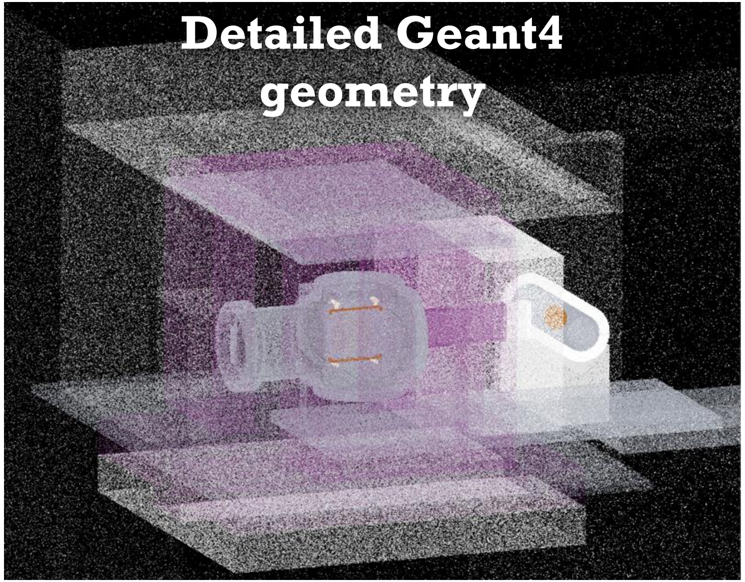

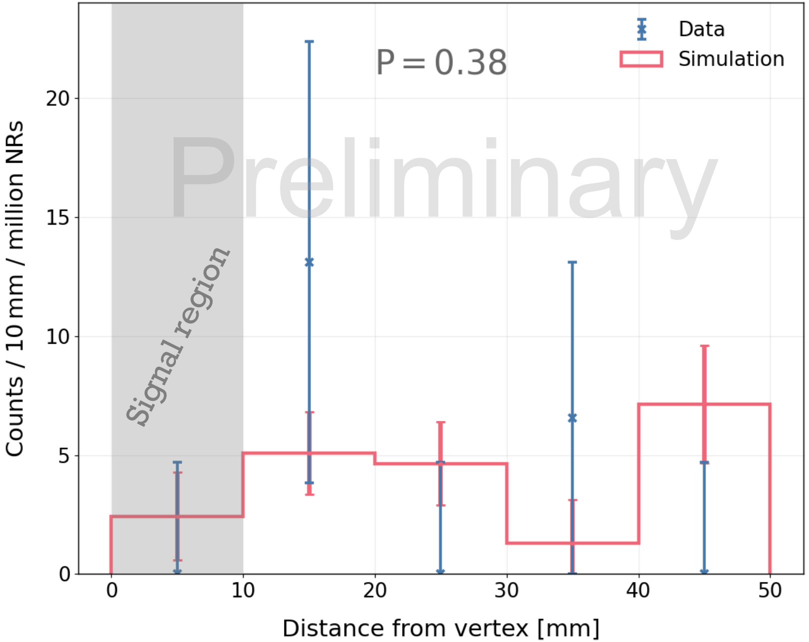

Beginning the search for Migdal with machine learning

- YOLOv8 is a state-of-the-art object detection algorithm.
- Object detection simultaneously classifies and localizes (with bounding boxes) any number of objects of interest in an image.
- Pipeline provides online deliverables, including mixed-field particle ID and NR energy spectra in real time.

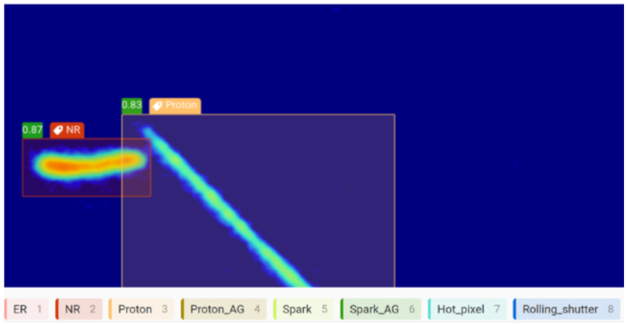

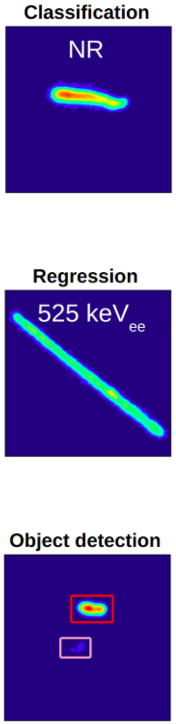

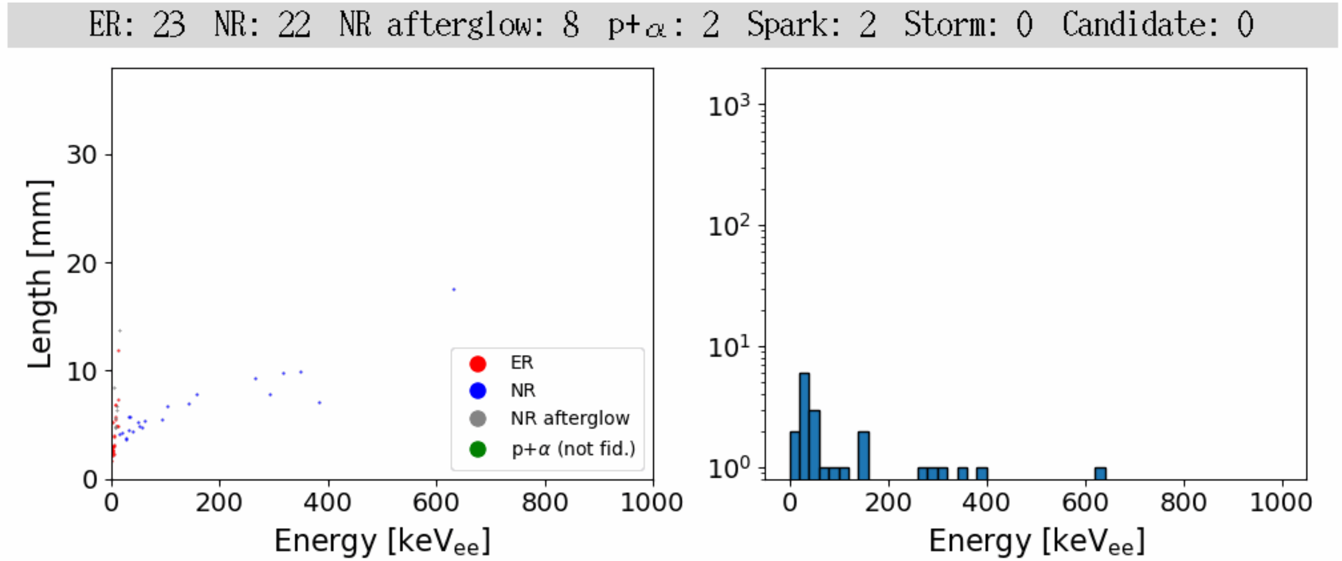

(arXiv.2406.07538)

Beginning the search for Migdal with machine learning

- YOLOv8 is a state-of-the-art object detection algorithm.
- Object detection simultaneously classifies and localizes (with bounding boxes) any number of objects of interest in an image.
- Pipeline provides online deliverables, including mixed-field particle ID and NR energy spectra in real time.

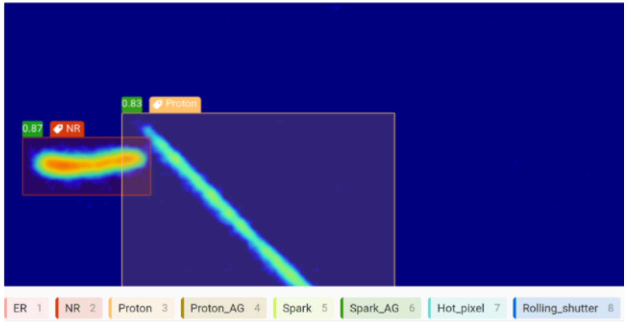

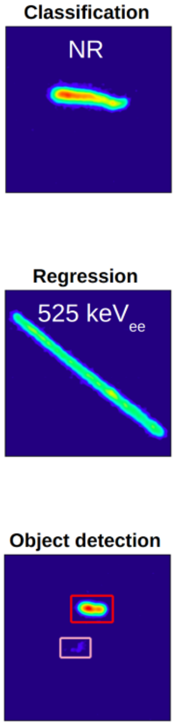

ER: 689 NR: 361 NR afterglow: 243 p+α: 69 Spark: 17 Storm: 0 Candidate: 0

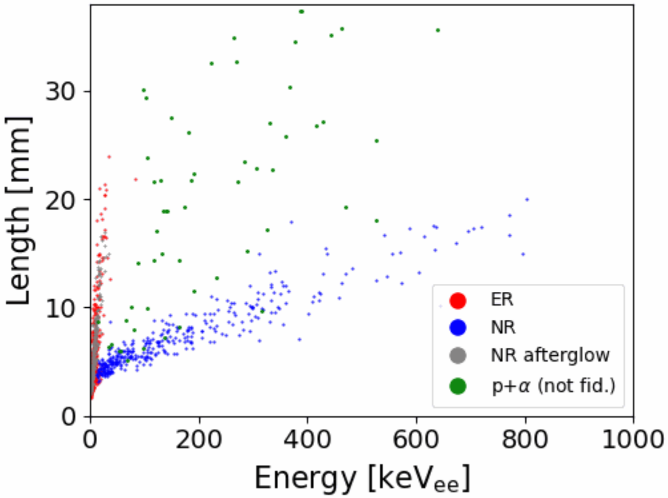

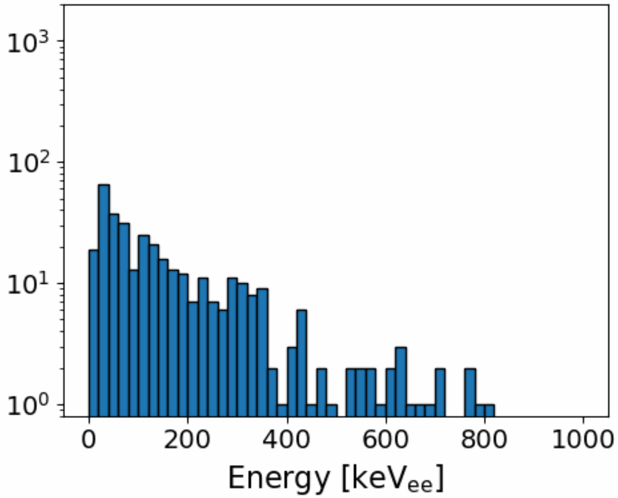

(arXiv.2406.07538)

Beginning the search for Migdal with machine learning

- YOLOv8 is a state-of-the-art object detection algorithm.
- Object detection simultaneously classifies and localizes (with bounding boxes) any number of objects of interest in an image.
- Pipeline provides online deliverables, including mixed-field particle ID and NR energy spectra in real time.

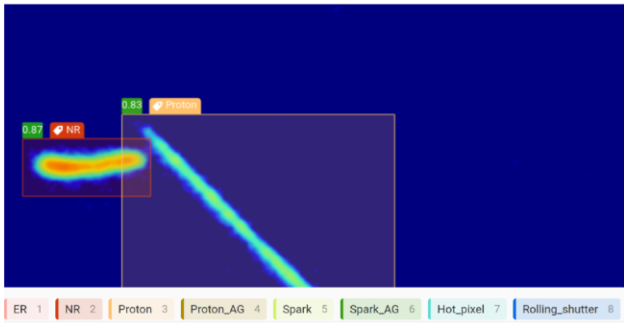

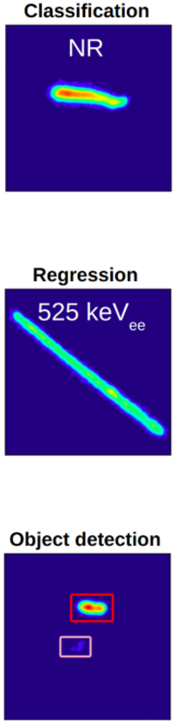

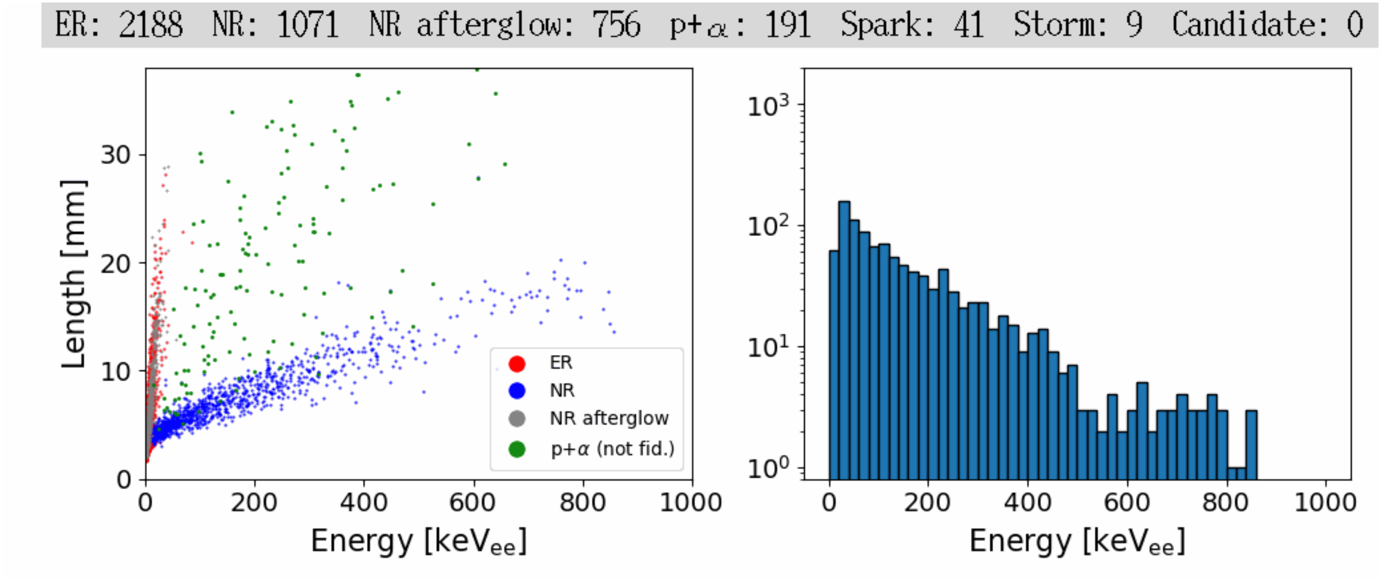

(arXiv.2406.07538)

Beginning the search for Migdal with machine learning

- YOLOv8 is a state-of-the-art object detection algorithm.
- Object detection simultaneously classifies and localizes (with bounding boxes) any number of objects of interest in an image.
- Pipeline provides online deliverables, including mixed-field particle ID and NR energy spectra in real time.

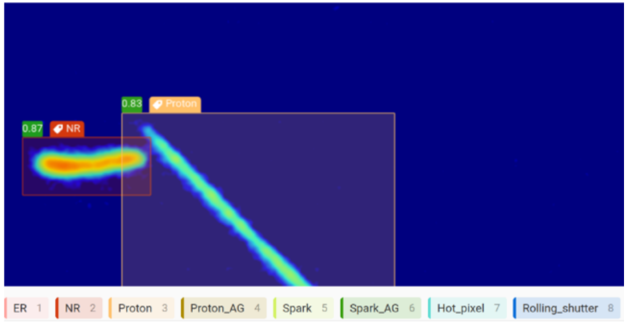

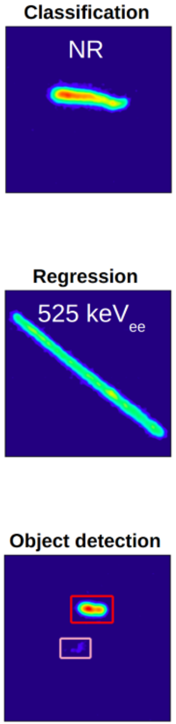

ER: 2967 NR: 1442 NR afterglow: 1009 p+α: 234 Spark: 60 Storm: 9 Candidate: 0

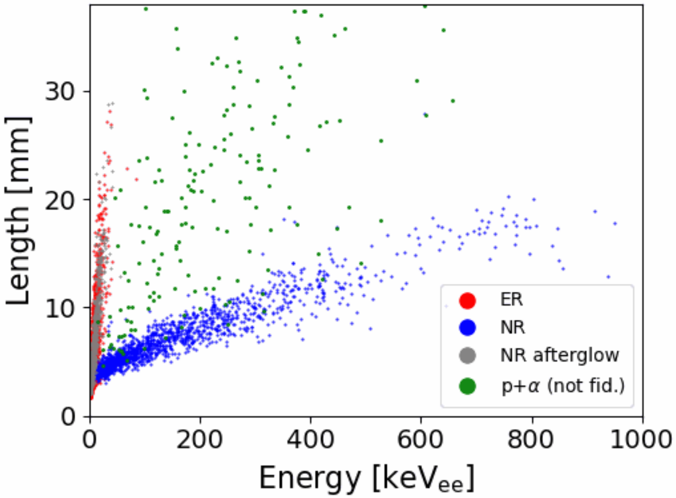

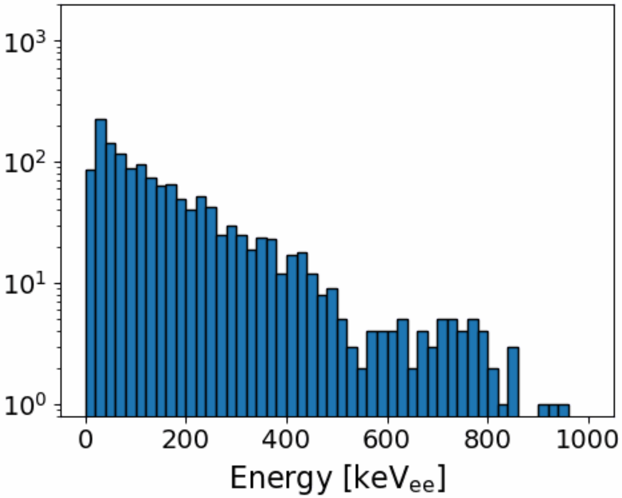

(arXiv.2406.07538)

Beginning the search for Migdal with machine learning

- YOLOv8 is a state-of-the-art object detection algorithm.
- Object detection simultaneously classifies and localizes (with bounding boxes) any number of objects of interest in an image.
- Pipeline provides online deliverables, including mixed-field particle ID and NR energy spectra in real time.

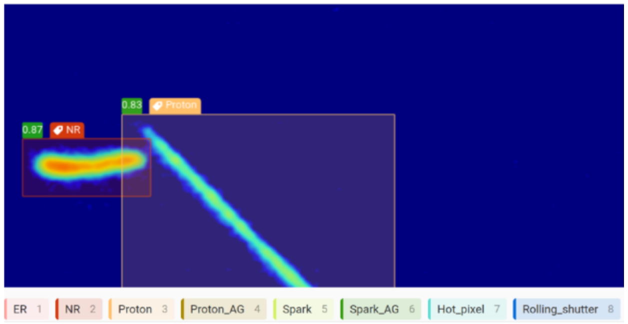

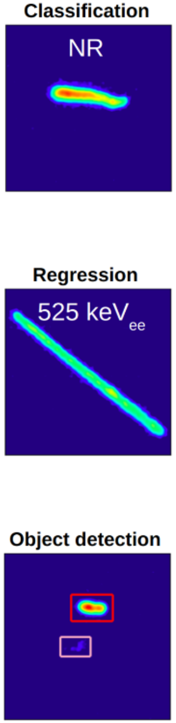

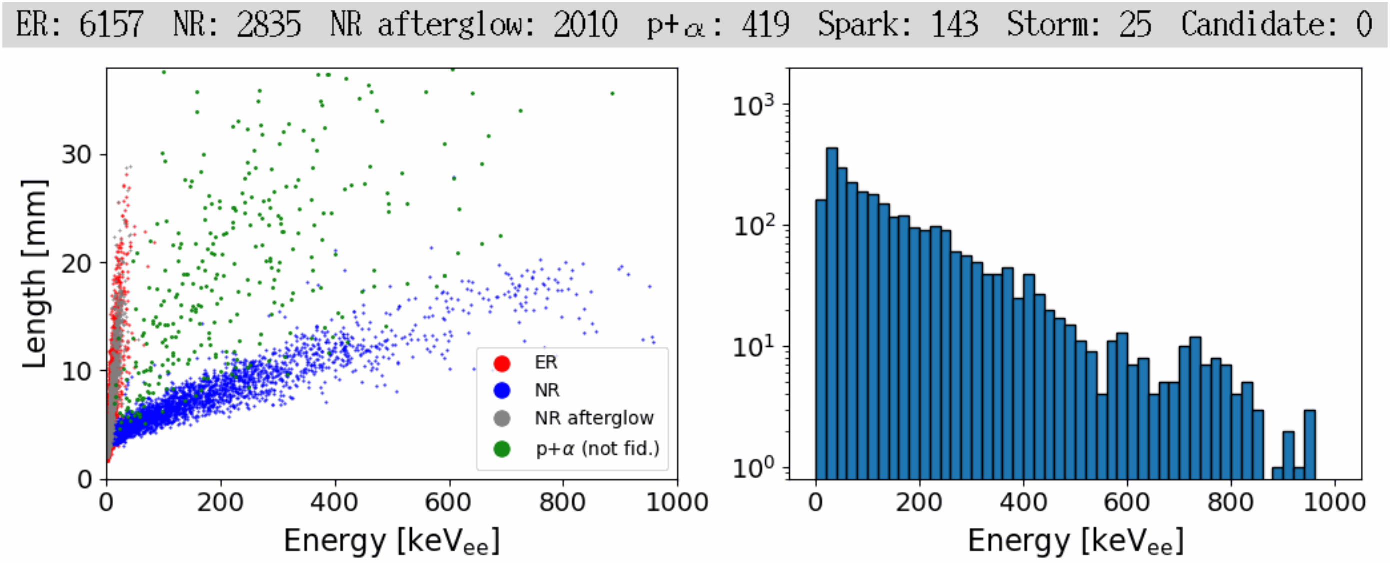

(arXiv.2406.07538)

Beginning the search for Migdal with machine learning

- YOLOv8 is a state-of-the-art object detection algorithm.
- Object detection simultaneously classifies and localizes (with bounding boxes) any number of objects of interest in an image.
- Pipeline provides online deliverables, including mixed-field particle ID and NR energy spectra in real time.

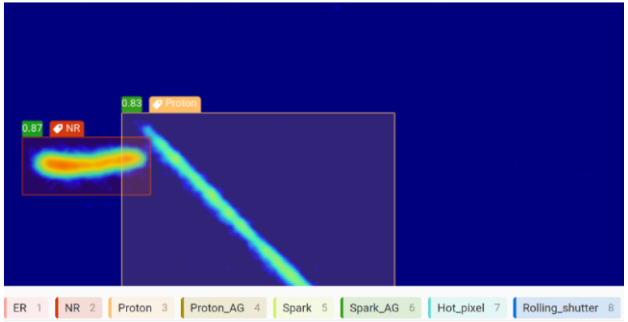

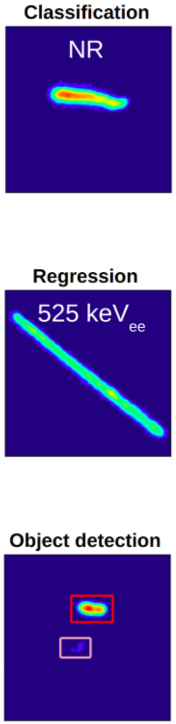

ER: 9180 NR: 4186 NR afterglow: 2958 p+α: 650 Spark: 220 Storm: 29 Candidate: 3

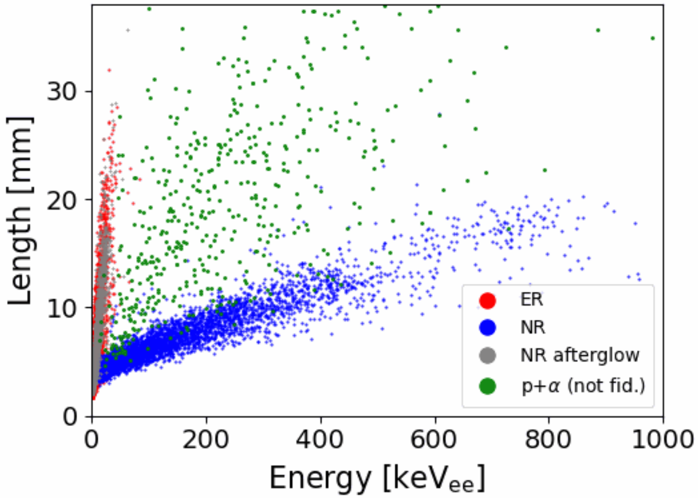

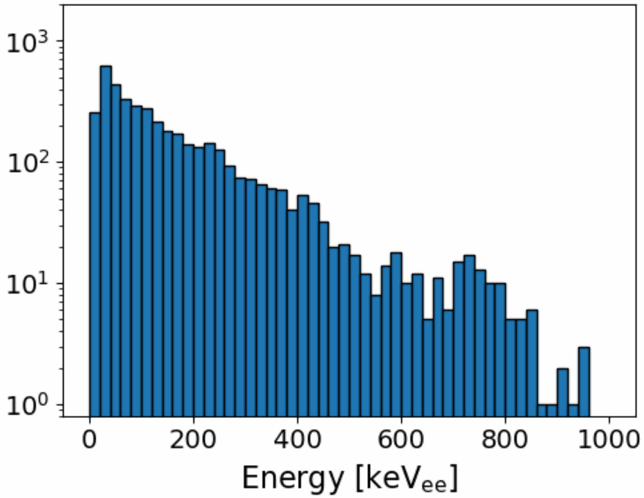

(arXiv.2406.07538)

Beginning the search for Migdal with machine learning

- YOLOv8 is a state-of-the-art object detection algorithm.
- Object detection simultaneously classifies and localizes (with bounding boxes) any number of objects of interest in an image.
- Pipeline provides online deliverables, including mixed-field particle ID and NR energy spectra in real time.

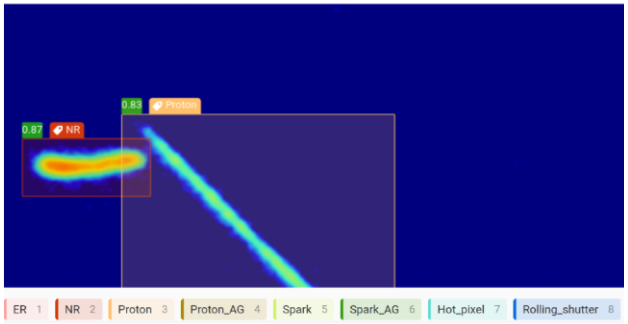

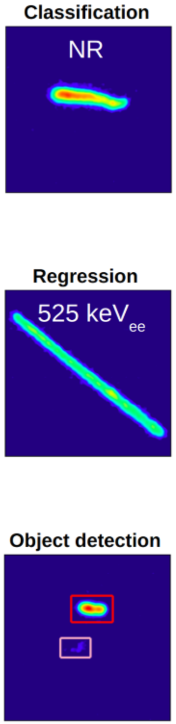

ER: 12310 NR: 5610 NR afterglow: 4024 p+α: 873 Spark: 299 Storm: 40 Candidate: 4

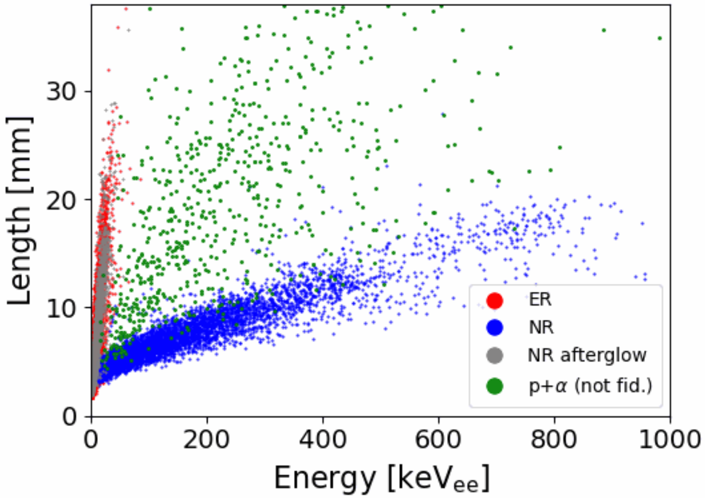

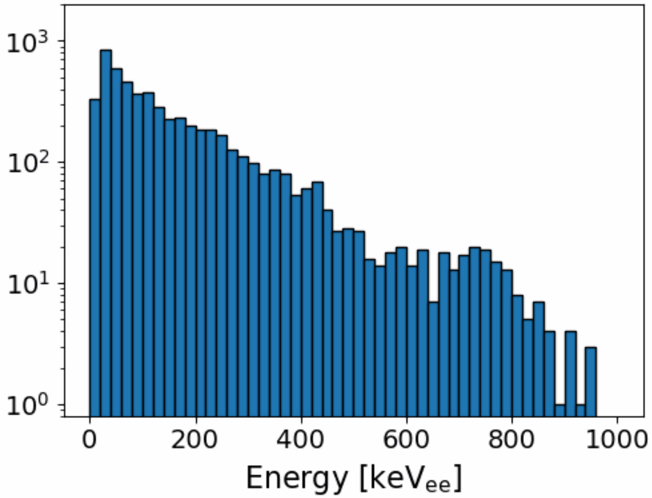

(arXiv.2406.07538)

Beginning the search for Migdal with machine learning

- YOLOv8 is a state-of-the-art object detection algorithm.
- Object detection simultaneously classifies and localizes (with bounding boxes) any number of objects of interest in an image.
- Pipeline provides online deliverables, including mixed-field particle ID and NR energy spectra in real time.

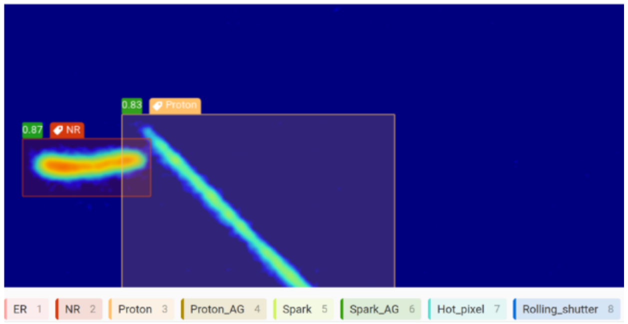

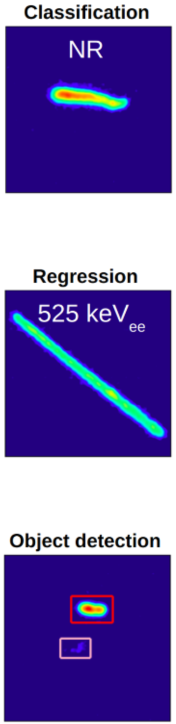

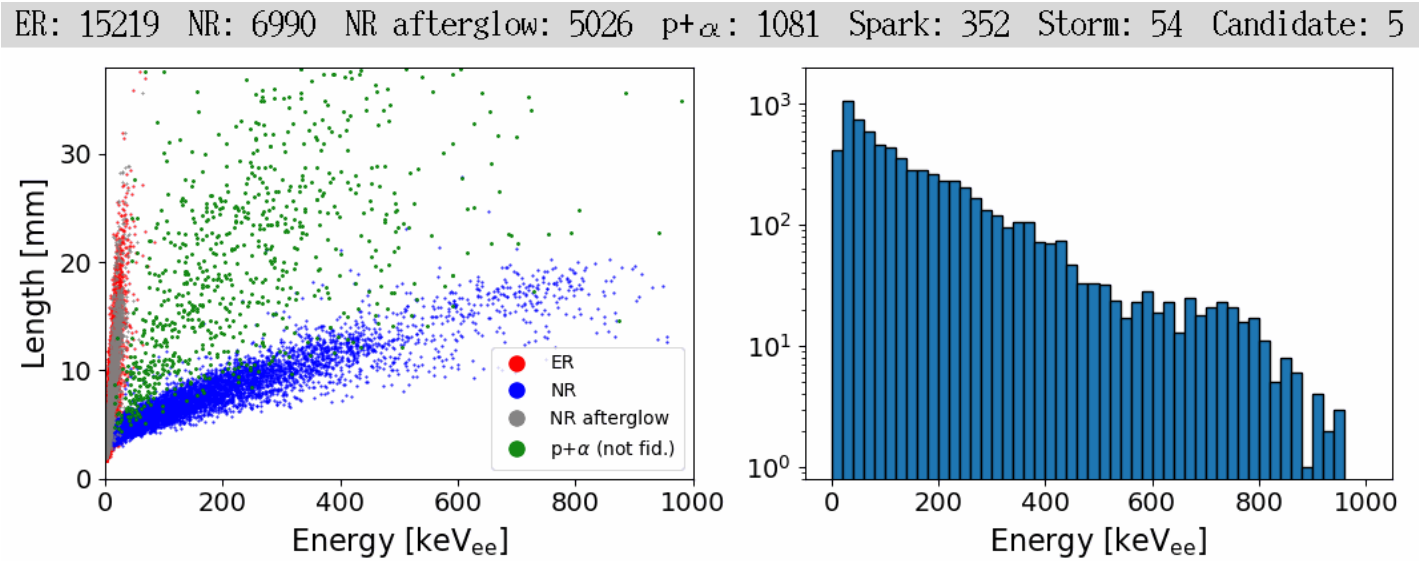

(arXiv.2406.07538)

YOLOv8 for data reduction

- YOLO currently operates on the images from the camera subsystem.
- YOLO finds several ERs within the vicinity of NRs.
- Keeping only frames with a single ER and NR within 6 mm of each other reduces a sample of **20 million frames** to **1,641**.
- Are these all Migdal? **No.**
- Camera exposure time (8.33 ms) is long enough for (few) events to pileup.
- We can resolve this with the ITO subsystem.

6 randomly chosen events from a sample of ERs + NRs with centroid distance < 6 mm

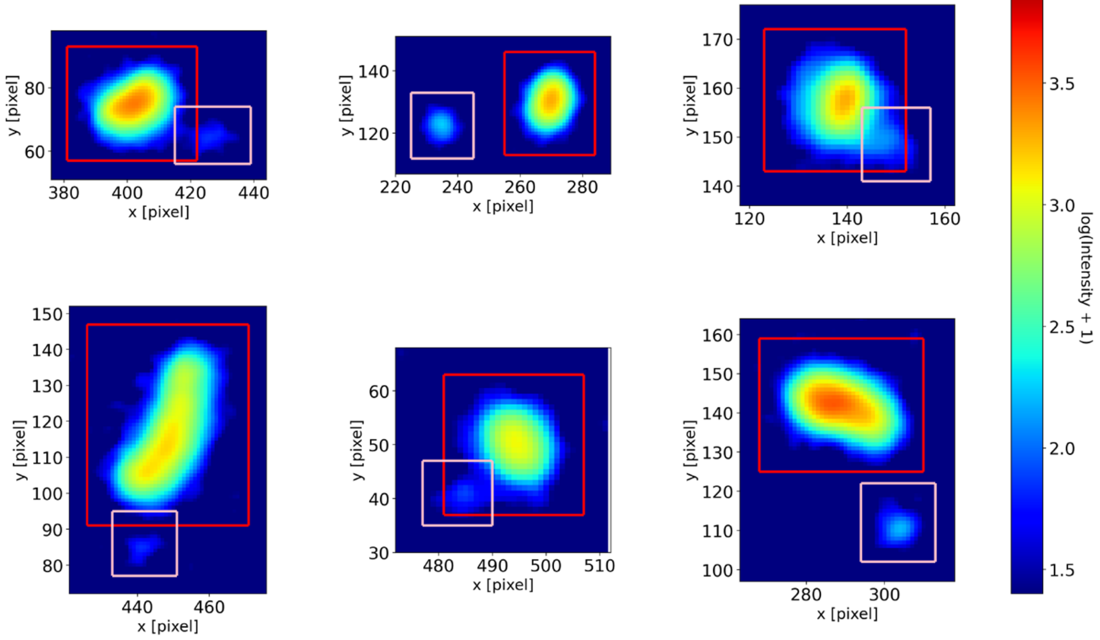

(arXiv.2406.07538)

Camera coincidences rejected in ITO

- The ITO's 2ns timing resolution allows for separation of events that pileup due to the camera's 8.33ms exposure time.
- The example on the right looks Migdal-like in the camera.
- In the ITO we see **these are two separate events** which occurred ~few ms apart.
- The ITO is vital for rejecting these coincidences.
  - If an event does not appear in the ITO, we reject it outright as a coincidence.

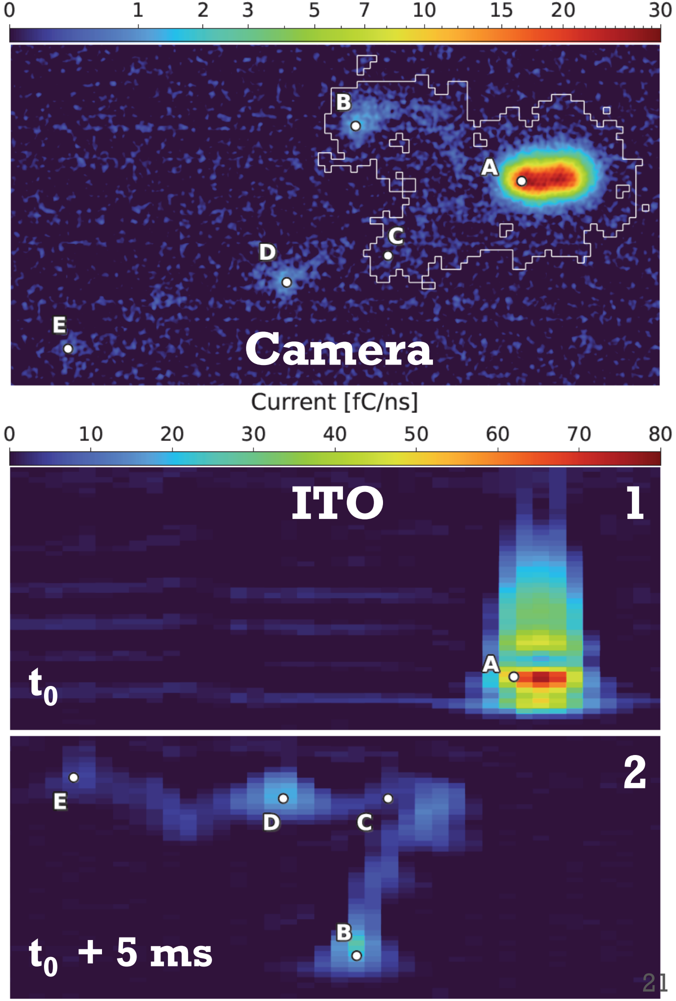

Summary

MIGDAL
Migdal In Galactic Dark mAtter expLoration

- The MIGDAL experiment aims to perform an unambiguous observation of the Migdal effect.
- Perpendicular optical and charge based planar readouts are combined to achieve 3D reconstruction of tracks.
- The detector is performing as designed.
- We have acquired several weeks of stable DD data. We will collect more.
- Data analysis of the two science runs is ongoing (stay tuned).
- Potential backgrounds appear to be as expected.
- YOLOv8 object identification allows fast feedback and event selection (arXiv.2406.07538).

Science and Technology Facilities Council
U.S. DEPARTMENT OF ENERGY
FCT Fundação para a Ciência e a Tecnologia
Horizon 2020 European Union Funding for Research & Innovation
National Science Foundation
MARIE CURIE ACTIONS

Backup

Papers

1. A. Migdal Ionizatsiya atomov pri yadernykh reaktsiyakh, ZhETF, 9, 1163-1165 (1939).
2. A. Migdal Ionizatsiya atomov pri α- i βraspade, ZhETF, 11, 207-212 (1941) .
3. M.S. Rapaport, F. Asaro and I. Pearlman Kshell electron shake-off accompanying alpha decay, PRC 11, 1740-1745 (1975).
4. M.S. Rapaport, F. Asaro and I. Pearlman L- and M-shell electron shake-off accompanying alpha decay, PRC 11, 1746-1754 (1975).
5. C. Couratin et al. , First Measurement of Pure Electron Shakeoff in the β Decay of Trapped 6He+ Ions, PRL 108, 243201 (2012).
6. X. Fabian et al., Electron Shakeoff following the β + decay of Trapped 19Ne+ and 35Ar+ trapped ions, PRA, 97, 023402 (2018).

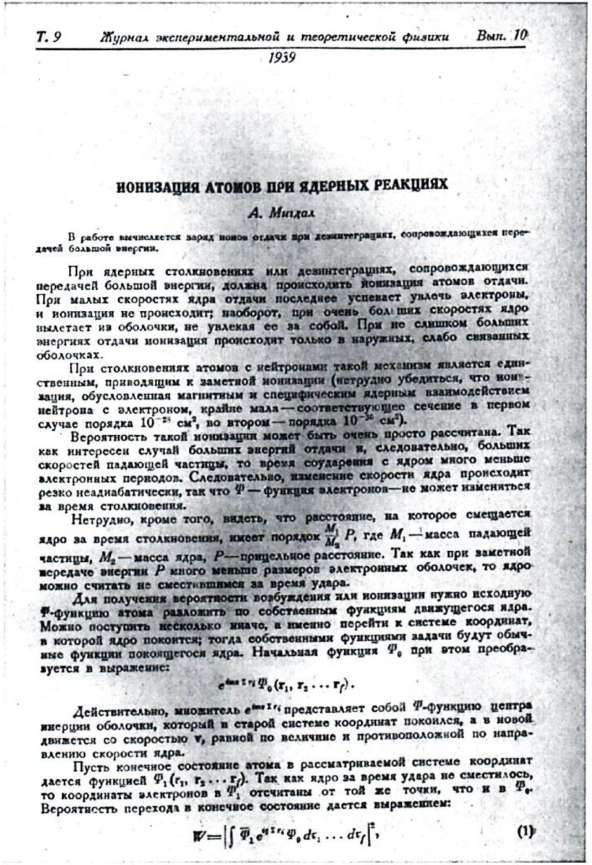

Т. 9 *Журнал экспериментальной и теоретической физики* Вып. 10
1939

ИОНИЗАЦИЯ АТОМОВ ПРИ ЯДЕРНЫХ РЕАКЦИЯХ

А. Мигдал

В работе вычисляется заряд ионов отдачи при дезинтеграциях, сопровождающихся передачей большой энергии.

При ядерных столкновениях или дезинтеграциях, сопровождающихся передачей большой энергии, должна происходить ионизация атомов отдачи. При малых скоростях ядра отдачи последнее успевает увлечь электроны, и ионизация не происходит; наоборот, при очень больших скоростях ядро вылетает из оболочки, не увлекая ее за собой. При не слишком больших энергиях отдачи ионизация происходит только в наружных, слабо связанных оболочках.

При столкновениях атомов с нейтронами такой механизм является единственным, приводящим к заметной ионизации (нетрудно убедиться, что ионизация, обусловленная магнитным и специфическим ядерным взаимодействием нейтрона с электроном, крайне мала — соответствующее сечение в первом случае порядка 10^{-28} см^2, во втором — порядка 10^{-36} см^2).

Вероятность такой ионизации может быть очень просто рассчитана. Так как интересен случай больших энергий отдачи и, следовательно, больших скоростей падающей частицы, то время соударения с ядром много меньше электронных периодов. Следовательно, изменение скорости ядра происходит резко неадиабатически, так что Ψ — функция электронов — не может измениться за время столкновения.

Нетрудно, кроме того, видеть, что расстояние, на которое смещается ядро за время столкновения, имеет порядок $\frac{M_1}{M_2}P$, где M_1 — масса падающей частицы, M_2 — масса ядра, P — прицельное расстояние. Так как при заметной передаче энергии P много меньше размеров электронных оболочек, то ядро можно считать не сместившимся за время удара.

Для получения вероятности возбуждения или ионизации нужно исходную Ψ-функцию атома разложить по собственным функциям движущегося ядра. Можно поступить несколько иначе, а именно перейти к системе координат, в которой ядро покоится; тогда собственными функциями задачи будут обычные функции покоящегося ядра. Начальная функция Ψ_0 при этом преобразуется в выражение:

$$e^{im\mathbf{v}\Sigma r_i}\Psi_0(\mathbf{r}_1, \mathbf{r}_2 \ldots \mathbf{r}_f).$$

Действительно, множитель $e^{im\mathbf{v}\Sigma r_i}$ представляет собой Ψ-функцию центра инерции оболочки, который в старой системе координат покоился, а в новой движется со скоростью $\mathbf{v}$, равной по величине и противоположной по направлению скорости ядра.

Пусть конечное состояние атома в рассматриваемой системе координат дается функцией $\Psi_1(\mathbf{r}_1, \mathbf{r}_2 \ldots \mathbf{r}_f)$. Так как ядро за время удара не сместилось, то координаты электронов в Ψ_1 отсчитаны от той же точки, что и в Ψ_0. Вероятность перехода в конечное состояние дается выражением:

$$W = \left|\int \overline{\Psi}_1 e^{iq\Sigma r_i}\Psi_0\, d\tau_1 \ldots d\tau_f\right|^2, \quad (1)$$

CF4 nuclear recoil spectrum & Migdal rates

- Higher rate of NRs at lower energies (Astropart. Phys. 151 (2023) 102853).
- Higher rate of Migdal events at higher energies (fluorine kinematic end-point).

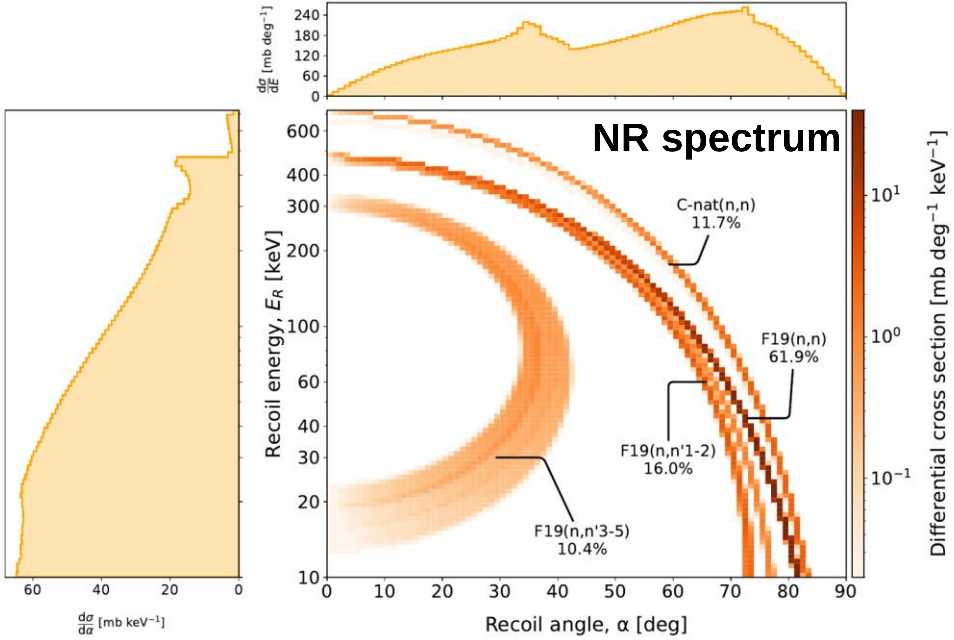

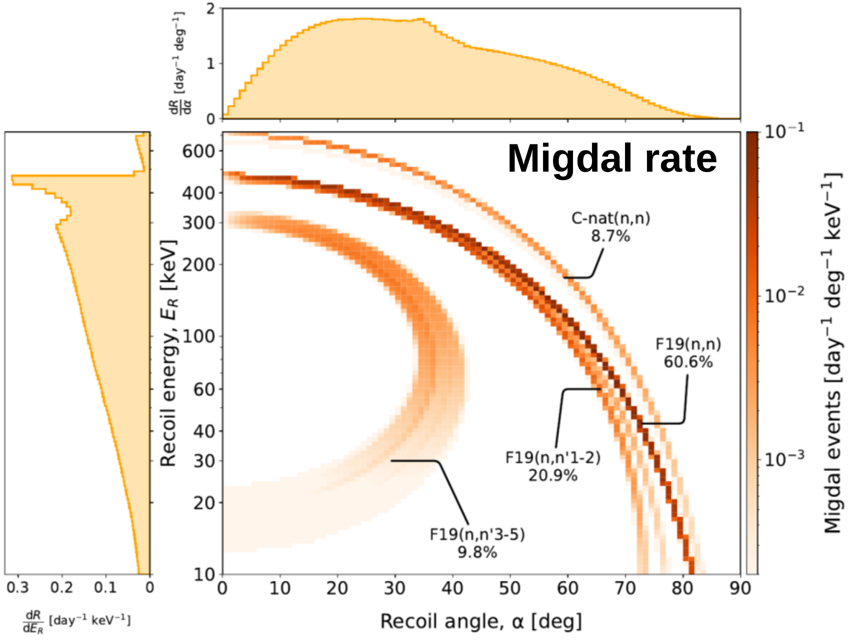

*per day at nominal neutron rate

Assembly at NILE

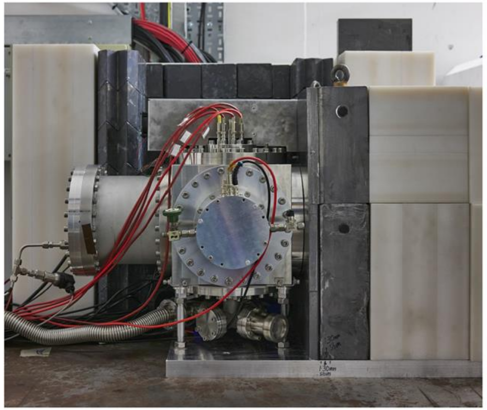

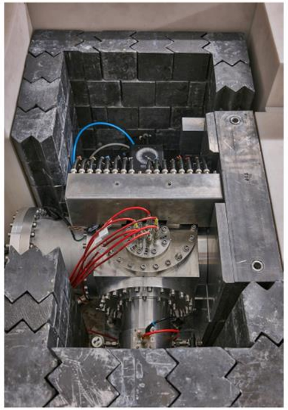

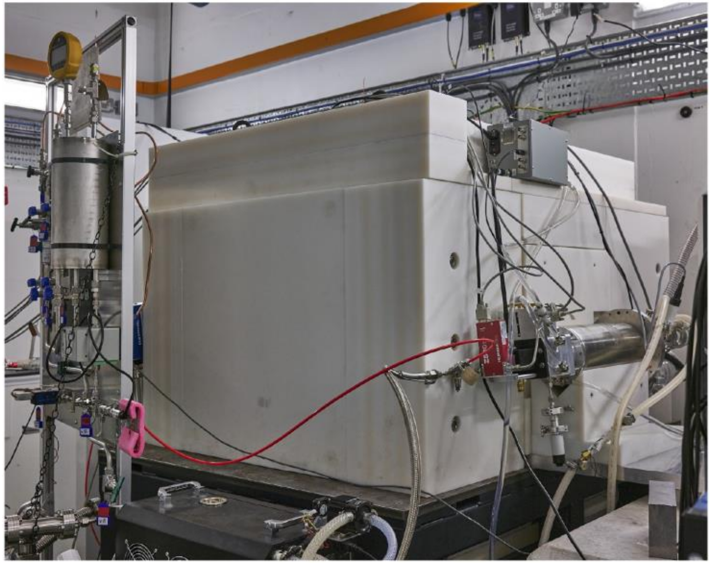

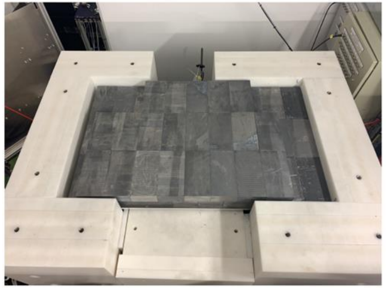

PMT

- The PMT is used to trigger the DAQ (on S2 signal) and obtain an absolute depth coordinate.
- The depth is calculated from the S1-S2 Δt and the drift velocity in the gas.
- PMT is digitised at 2 ns with 8-bit resolution.

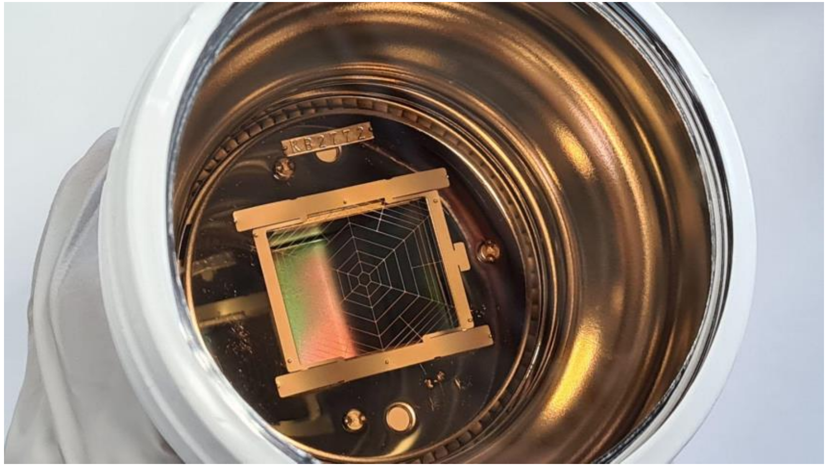

Hamamatsu R11410 PMT

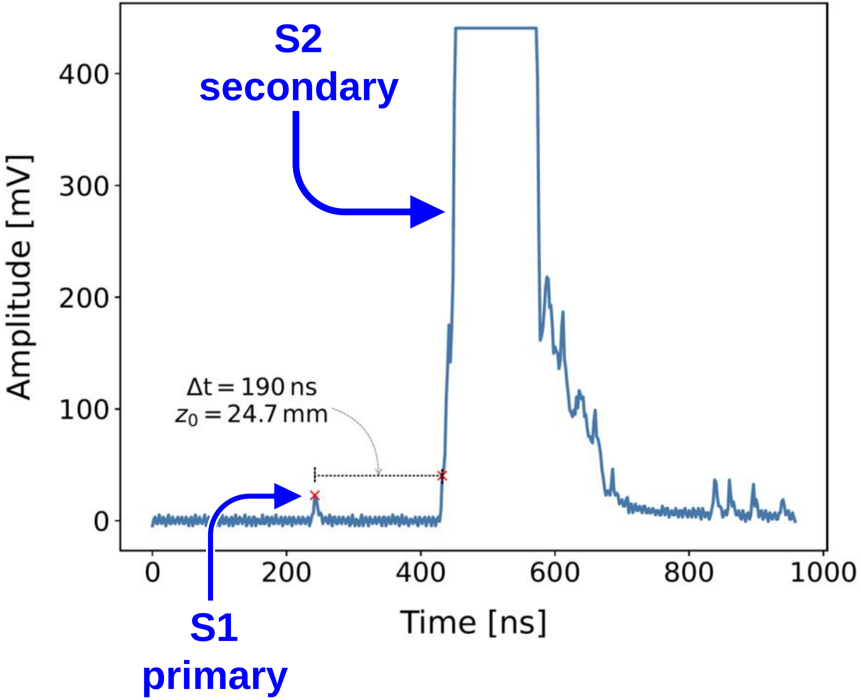

GEM mask

- Avoid tracks falling outside the camera field of view by attaching a mask to the TPC.
- This blocks NRs from being amplified outside the 80 x 45 mm^2 camera area.
- The ITO readout now sees the same active area as the camera.
- We also have a 100 x 60 mm^2 mask.
    - We plan to test this configuration soon.

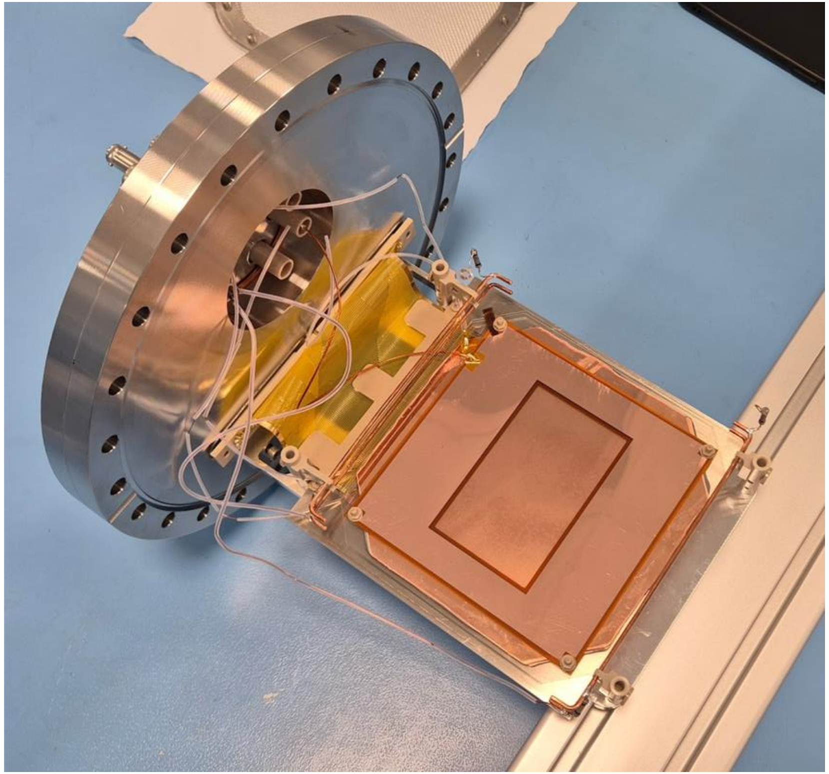

Optical distortion correction

- We characterise the distortion by imaging a regular grid and measuring the deflection of the lines as a function of radial distance.
- Barrel distortion in the camera can be parameterised by a 5^{th}-order polynomial.
- Imaging closer to the focal plane increases distortion.

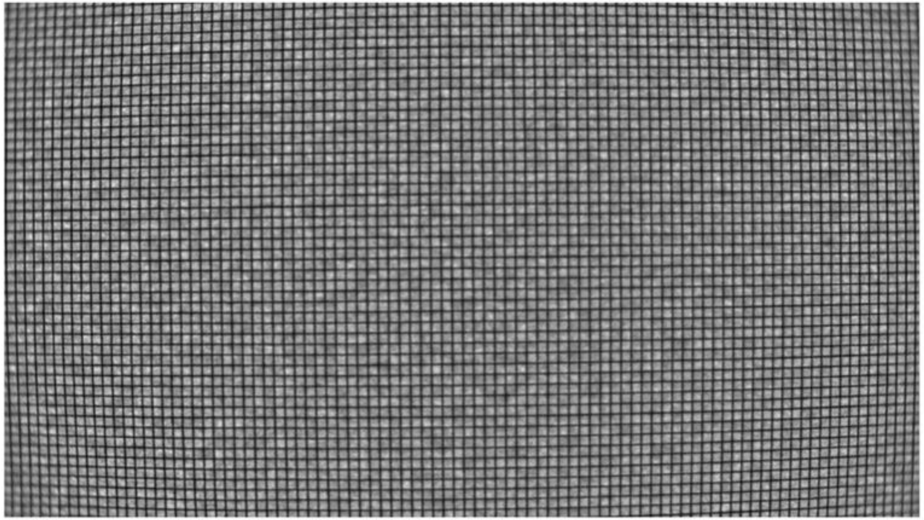

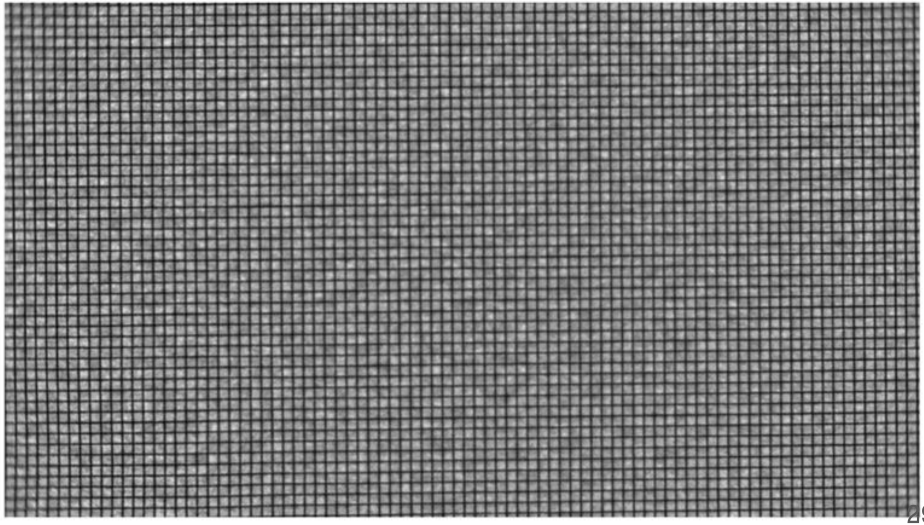

Flat field correction in the camera

- We use an ^{55}Fe source as an energy calibration.
- Interactions occur over the entire volume, so we can perform a position-dependent calibration.
- Below is a map of the relative intensities of ^{55}Fe events.

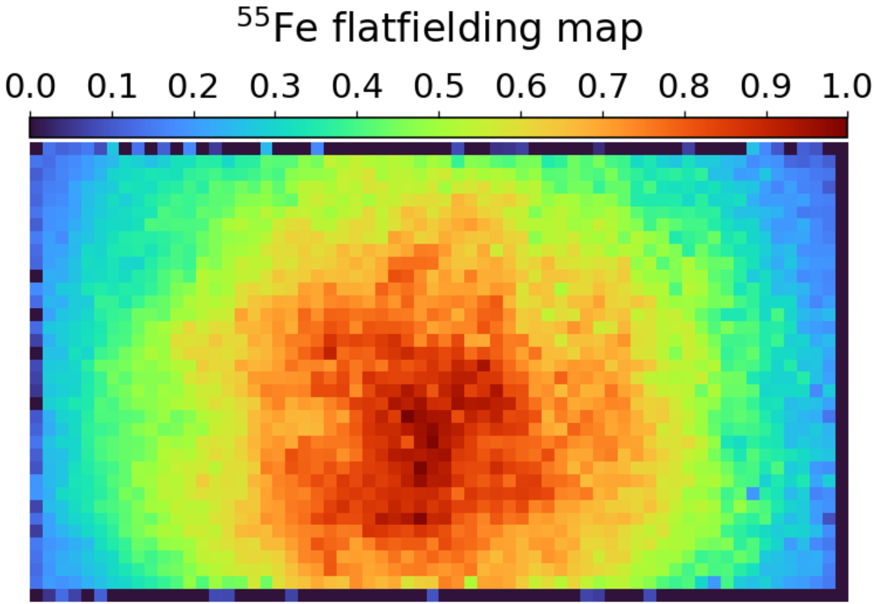

Capabilities of the ORCA Quest

- The ORCA Quest is capable of ‘photon-number resolving’ at the cost of a slower, 5 Hz readout rate.
- Using this mode risks pileup of events, only useful for low-noise calibration.

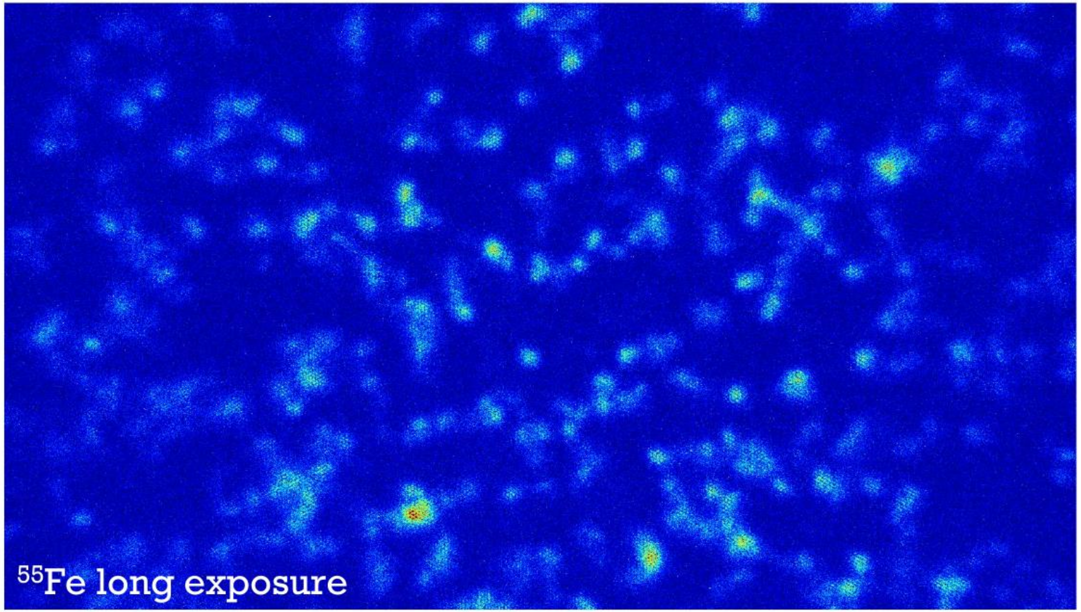

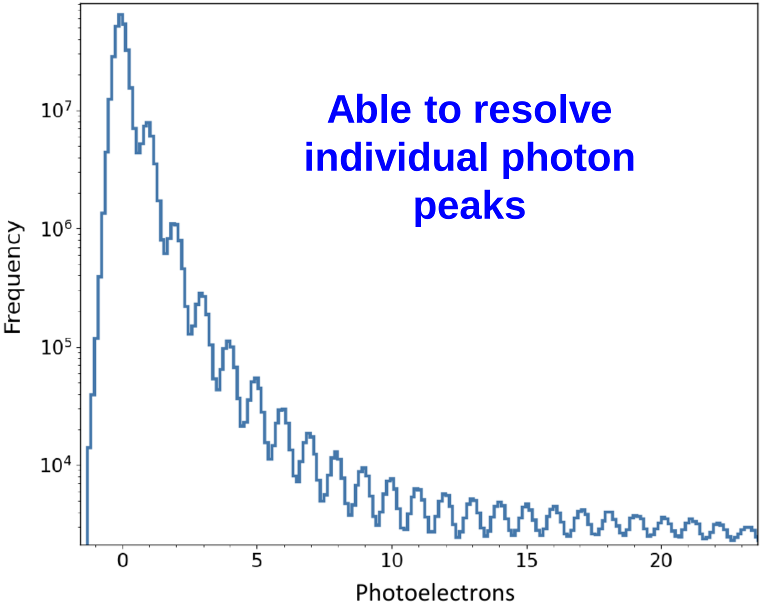

Camera afterglow

- The ORCA Quest appears to feature an ‘afterglow’ in the subsequent frame following bright events.
- In the frame which follows each high-energy track, we see an afterglow of ~1 photoelectron in many pixels.
- **This appears to be a persistence for {N} frames, rather than {T} exposure time.**
- We can simply mask bright areas in the subsequent frame to avoid confusion.

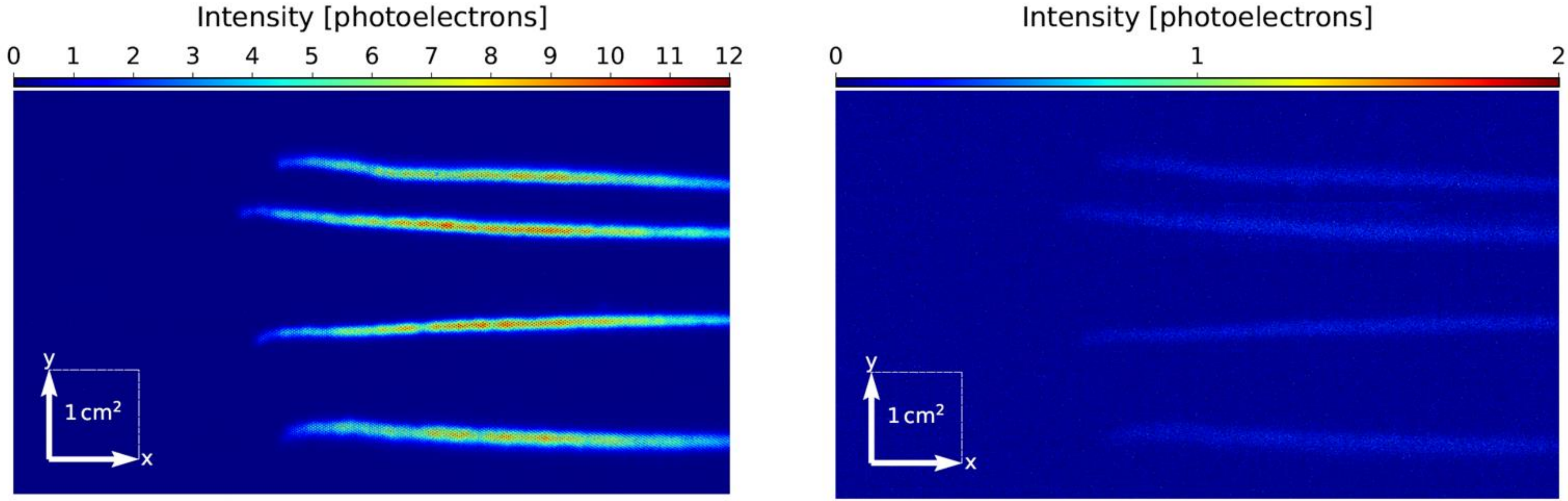

Glass GEM considerations

- Light can refract in the glass substrate and reflect on the copper surfaces.
- We experience a continuous reduction in the gas gain while operating with highly ionising particles, requires regular voltage adjustment to maintain gain.

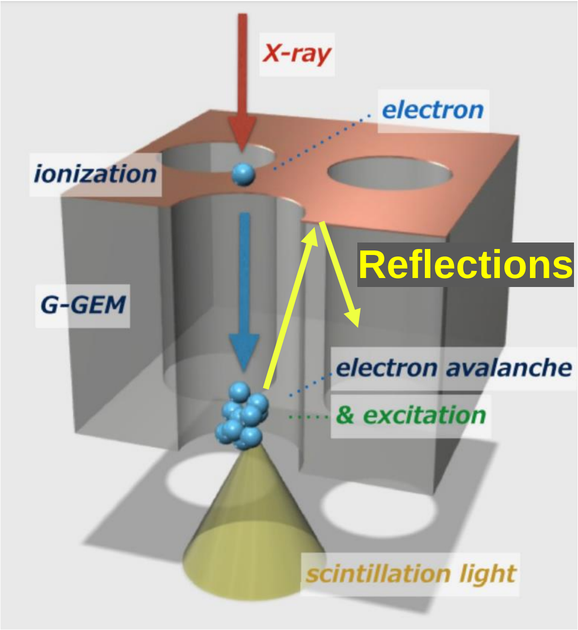

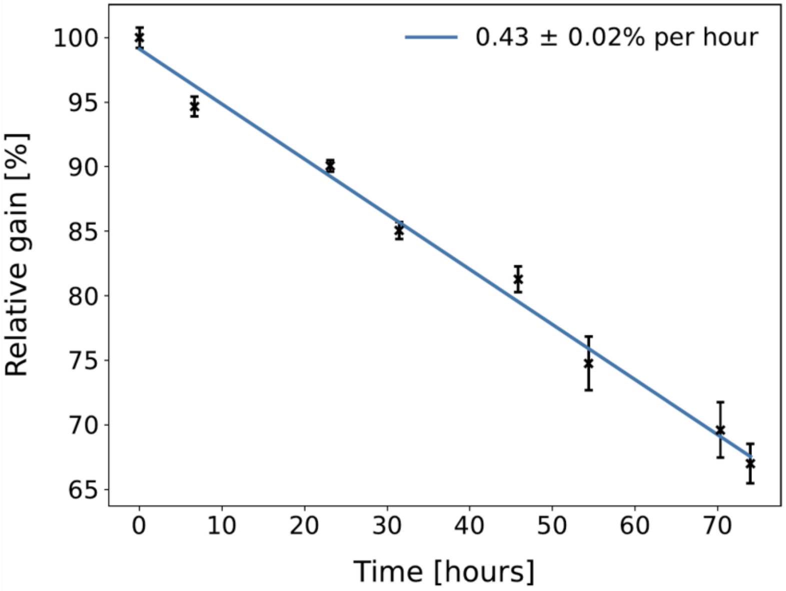

Noble gas mixtures

- We plan to operate with DD neutrons in a fraction of argon gas later in 2024.

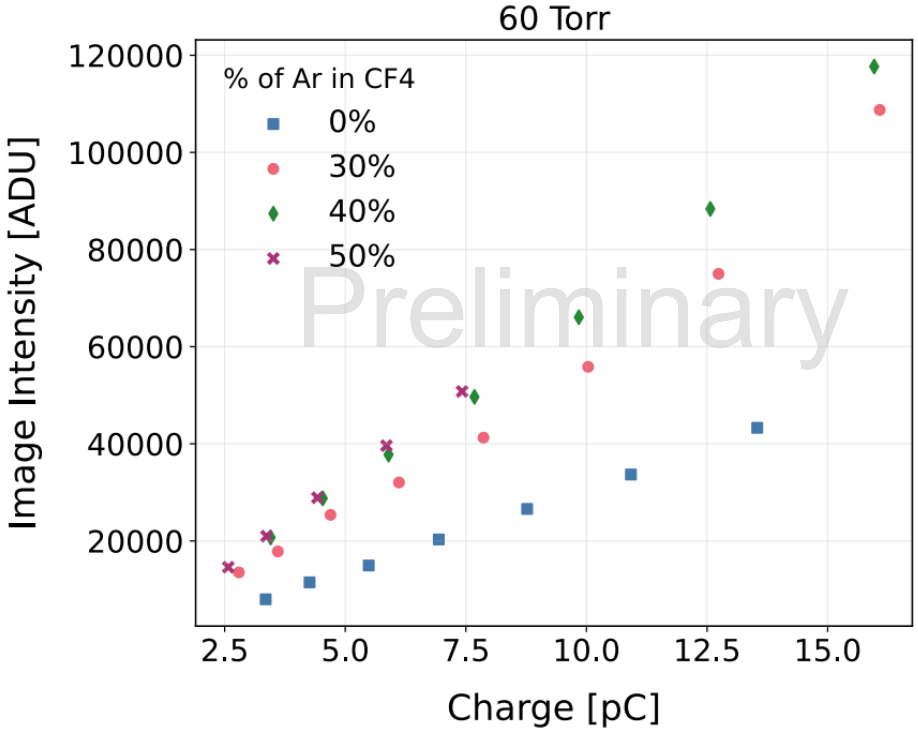

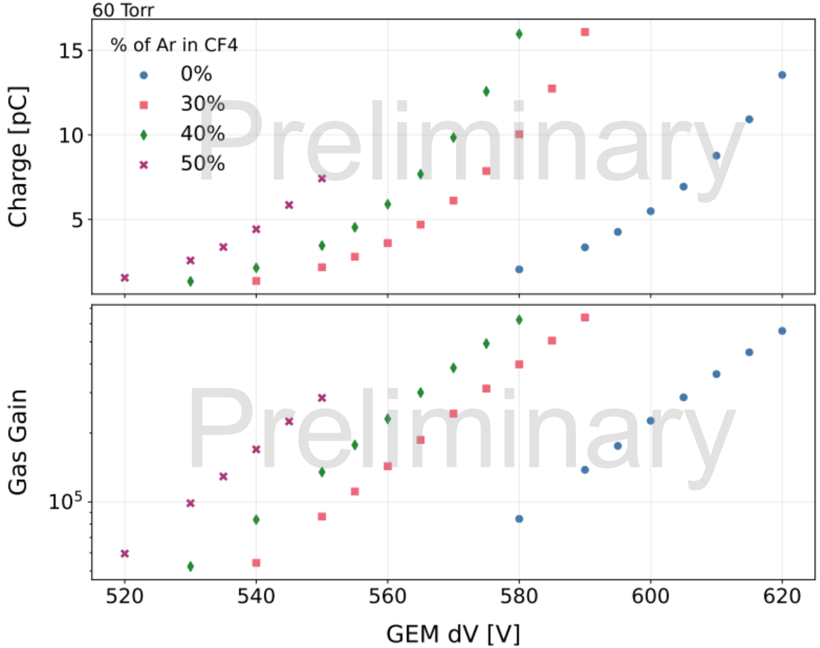

Light yield enhanced with addition of Ar.

L. Millins (MIGDAL),
16th Pisa Meeting on Advanced Detectors

May 31 2024, Isola d'Elba

MIGDAL upgrade

- Higher resolution digitiser (CAEN V1730).
  - 14-bit instead of 8-bit.
- Doubling the number of ITO strips to 240, increasing spatial resolution in the ITO subsystem.
  - 0.417 mm instead of 0.833 mm.
- Additional amplification stage.
  - Testing addition of a third GEM (kapton, glass, or ceramic).
  - Testing different structures (M-ThGEMs).
- Reduction of reflections.
  - Opaque GEMs.
  - Considering dark-coating TPC.